Ice-Shelf Melt Response to Changing Winds and Glacier Dynamics in the Amundsen Sea Sector, Antarctica

Marion Donat-magnin, Nicolas Jourdain, Paul Spence, Julien Le Sommer, Hubert Gallée, Gaël Durand

AGU PUBLICATIONS

JGR

Journal of Geophysical Research: Oceans

RESEARCH ARTICLE

10.1002/2017JC013059

Ice-Shelf Melt Response to Changing Winds and Glacier Dynamics in the Amundsen Sea Sector, Antarctica

Marion Donat-Magnin[1], Nicolas C. Jourdain[1], Paul Spence[2], Julien Le Sommer[1], Hubert Gallée[1], and Gaël Durand[1]

[1]Université Grenoble Alpes/CNRS/IRD/G-INP, IGE, Grenoble, France, [2]ARC Centre of Excellence for Climate System Science, University of New South Wales, Sydney, NSW, Australia

Key Points:
- The simulated coastal ocean response to changing winds is strongly impacted by the circulation induced by ice-shelf melt
- Strengthening and poleward shifting winds significantly affect simulated melt rates underneath Pine Island and Thwaites
- The simulated melt rates considerably evolve during an extreme grounding line retreat, which emphasizes the need for coupled ocean-ice sheet models

Correspondence to:
M. Donat-Magnin,
marion.donatmagnin@gmail.com

Citation:
Donat-Magnin, M., Jourdain, N. C., Spence, P., Le Sommer, J., Gallée, H., & Durand, G. (2017). Ice-shelf melt response to changing winds and glacier dynamics in the Amundsen Sea Sector, Antarctica. *Journal of Geophysical Research: Oceans*, *122*, 10,206–10,224. https://doi.org/10.1002/2017JC013059

Received 4 MAY 2017
Accepted 27 NOV 2017
Accepted article online 6 DEC 2017
Published online 29 DEC 2017

Abstract It has been suggested that the coastal Southern Ocean subsurface may warm over the 21st century in response to strengthening and poleward shifting winds, with potential adverse effects on West Antarctic glaciers. However, using a 1/12° ocean regional model that includes ice-shelf cavities, we find a more complex response to changing winds in the Amundsen Sea. Simulated offshore subsurface waters get colder under strengthened and poleward shifted winds representative of the SAM projected trend. The buoyancy-driven circulation induced by ice-shelf melt transports this cold offshore anomaly onto the continental shelf, leading to cooling and decreased melt below 450 m. In the vicinity of ice-shelf fronts, Ekman pumping contributes to raise the isotherms in response to changing winds. This effect overwhelms the horizontal transport of colder offshore waters at intermediate depths (between 200 and 450 m), and therefore increases melt rates in the upper part of the ice-shelf cavities, which reinforces the buoyancy-driven circulation and further contributes to raise the isotherms. Then, prescribing an extreme grounding line retreat projected for 2100, the total melt rates simulated underneath Thwaites and Pine Island are multiplied by 2.5. Such increase is explained by a larger ocean/ice interface exposed to CDW, which is then amplified by a stronger melt-induced circulation along the ice draft. Our main conclusions are that (1) outputs from ocean models that do not represent ice shelf cavities (e.g., CMIP5 models) should not be directly used to predict the thermal forcing of future ice shelf cavities; (2) coupled ocean/ice sheet models with a velocity-dependent melt formulation are needed for future projections of glaciers experiencing a significant grounding line retreat.

1. Introduction

Changing oceanic melt underneath ice-shelves is suspected to trigger glacier acceleration and ice-sheet instability in West Antarctica (Favier et al., 2014; Joughin et al., 2014; Schoof, 2007). In the Amundsen Sea sector, ocean-induced melting is likely responsible for the observed ice-shelves thinning and grounding line retreat (Jacobs et al., 2012; Joughin et al., 2010; Rignot et al., 2014; Seroussi et al., 2017; Turner et al., 2017). The outlet glaciers located in the Amundsen Sea have increased their ice flux through the grounding line by 77% over the last three to four decades (Mouginot et al., 2014). This makes the Amundsen glaciers the largest contributor to sea level rise in Antarctica (Shepherd et al., 2012).

Predictions of Antarctic contribution to sea level rise are usually performed with ice dynamics models. So far, a majority of these modeling studies empirically prescribe changes in melt rates profiles to assess the future evolution of Antarctic glaciers. This is done either by ad hoc modifications of simple analytical melt rate profiles (e.g., Favier et al., 2014; Joughin et al., 2014) or by parameterizing melt rates from temperature at the nearest climate model grid points (e.g., Cornford et al., 2015; Deconto & Pollard, 2016; Martin et al., 2011). These methods are not designed to account for complex feedbacks between ice draft shapes (depth of the ice-shelf base) and oceanic melt rates, and can lead to important errors in mass loss and grounding line retreat estimates (De Rydt & Gudmundsson, 2016; Seroussi et al., 2017). Moreover, parameterized melt rates reported in the literature have been derived from various kinds of temperature anomalies, e.g., sea surface temperature anomaly (Golledge et al., 2015), average subsurface (200–800 m) temperature anomaly (Cornford et al., 2015), or 400 m temperature anomaly (Deconto & Pollard, 2016). To date, there is no evidence that any of these methods is robust to represent trends in ice-shelf melt rates, and there is a strong need to better understand and simulate the response of ice-shelf melt to climatic forcings.

Variations of the coastal ocean subsurface properties around Antarctica have often been attributed to wind variations (Dinniman et al., 2011; Spence et al., 2014; Steig et al., 2012; Thoma et al., 2008). The leading mode of atmospheric circulation around Antarctica is the Southern Annular Mode (SAM, e.g., Thompson & Wallace, 2000). The SAM reflects the variability in intensity and position of surface westerly winds around Antarctica, in relation with the storm track and tropospheric jet dynamics (Hartmann & Lo, 1998; Limpasuvan & Hartmann, 1999). While the SAM is the leading mode for the entire Southern Ocean, other oscillations can also be important regionally, such as the Amundsen Sea Low (ASL) variability (e.g., Raphael et al., 2016) which is related to the SAM and to tropical variability (Fogt & Wovrosh, 2015; Turner et al., 2013). Over the last three to five decades, the SAM has encountered a positive trend, i.e., westerly winds have been strengthening and shifting poleward (Chen & Held, 2007; Jones et al., 2016; Marshall, 2003), while the ASL circulation has been strengthening (Raphael et al., 2016). The observed SAM trend is unusual compared to palaeoclimatological records over the last millennium, but there is currently no observational evidence that the ASL trend is distinct from natural variability (Jones et al., 2016). Most simulations from the fifth Coupled Model Intercomparison Project (CMIP5) predict strengthening and poleward shifting of westerly winds throughout the 21st century under the highest greenhouse gases emission scenario, partly compensated by stratospheric ozone recovery in the first half of the century (Bracegirdle et al., 2013; Gillett & Fyfe, 2013; Jones et al., 2016; Zheng et al., 2013). However, the CMIP5 models present strong biases over the Southern Ocean, with too weak and equatorward-biased westerly winds in most models (Bracegirdle et al., 2013, 2014; Swart & Fyfe, 2012).

Observed temperature profiles within the Antarctic Circumpolar Current (ACC) indicate a warming of the top 1,000 m over the 20th century, likely related to the aforementioned trends in surface winds (Gille, 2008). In contrast to the ACC region, it is currently difficult to identify trends in ocean temperatures near the Antarctic margins because measurements there have started recently and sparsely, in particular in the Amundsen Sea (e.g., Jacobs et al., 2012; Schmidtko et al., 2014). Such trend identification is nonetheless possible in climate simulations, which predict a warming of the ocean subsurface (below $\sim$200 m) along the Antarctic ice-sheet margins over the 21st century (Yin et al., 2011), and possibly persisting for centuries (Gillett et al., 2011). Such subsurface warming is consistent with the warming found offshore in the CMIP5 models in response to anthropogenic forcing (Sallée et al., 2013). Because of the aforementioned wind biases in most CMIP5 models, Spence et al. (2014) prescribed a bias-corrected SAM trend guided by 32 climate models and representative of a high-emission scenario in ocean global simulations. They found that the SAM-induced subsurface warming could be attributed to poleward shifting winds through changes in Ekman transport from the 20th to the end of 21st century. Other variabilities, such as ASL migrations (Thoma et al., 2008), Rossby wave trains from the tropical Pacific (Dutrieux et al., 2014; Steig et al., 2012), or Ekman induced on-shelf transports by along slope currents (Wåhlin et al., 2012), can affect the intraseasonal and interannual variability of oceanic heat supply to ice shelves in the Amundsen Sea, but there is currently no evidence that these variabilities will change ocean temperatures in response to anthropogenic forcing (Scambos et al., 2017). It is important to bear in mind that the aforementioned climate studies on the impact of the SAM trend on ocean temperatures do not include interactive ice-shelf cavities, i.e., melt rates neither respond to nor affect the ocean properties (which may be important according to Bintanja et al., 2013; Jourdain et al., 2017; Pauling et al., 2016; Swart & Fyfe, 2013) and the feedbacks between melt rates and the ice dynamics are not accounted for (which may be important according to De Rydt & Gudmundsson, 2016; Seroussi et al., 2017).

To summarize, the difficulty to estimate the ice-shelf melt response to anthropogenic forcing based on CMIP climate projections arises from several limitations: (1) the wind simulated by CMIP models is significantly biased, which casts doubt on the ocean changes in these simulations, and limits the evaluation of ocean/ice-shelf simulations directly forced by CMIP winds; (2) CMIP models do not represent the feedbacks between ice-shelf melt rates and the ocean properties; (3) CMIP models do not represent the feedbacks between ice-shelf melt and the ice dynamics. In this paper, we assess the importance of the second and the third limitations. We use a regional ocean model configuration of the Amundsen Sea that includes a representation of static ice-shelf cavities with interactive melt rates. We overcome the first aforementioned limitation by embedding our regional simulations into the global simulation from Spence et al. (2014) and its bias-corrected SAM trend. Our motivations to study the SAM trends are that the trend is projected to continue over the 21st century under strong emission scenarios with subsequent warming of the subsurface of

coastal Antarctic seas, and that the currently observed SAM trend is the only climate trend in Antarctica to be reported as unprecedented compared to paleorecords over the last few centuries. Our experimental design is described in section 2. The influence of ice-shelves on the ocean response to the SAM trend and the melt response to the SAM trend are analyzed in section 3.1. Finally, we estimate how changes in the shape of ice-shelf cavities can affect melt rates by imposing several geometries from the ice-dynamics simulations produced by Cornford et al. (2015) (section 3.2).

2. Material and Methods

To estimate the Amundsen Sea response to projected SAM changes, we use the global ocean simulations produced by Spence et al. (2014) accounting for both the present-day winds and the bias-corrected SAM change through the 21st century. To estimate potential feedbacks related to changes in ice dynamics, we make use of ice-sheet simulations over the 21st century produced by Cornford et al. (2015). Both of these published simulations are used to constrain our regional ocean simulations and are therefore described in section 2.1. Then, our regional ocean model configuration of the Amundsen Sea is described in section 2.2, together with a list of our experiments.

2.1. Imposed Climatic Perturbations

Our present-day atmosphere and global ocean (i.e., at the boundaries of our regional domain) are from Spence et al. (2014) who produced a 0.25° global ocean simulations constrained by the CORE-II Normal Year Forcing (NYF, Griffies et al., 2009; Large & Yeager, 2009). CORE-II-NYF includes synoptic variability but does not include interannual variability. While this prevents us from studying the observed year-to-year variability as in St-Laurent et al. (2015) and Nakayama et al. (2017), it was important to use an atmospheric forcing data set consistent with the simulations of Spence et al. (2014) which are here downscaled. We also acknowledge that CORE-II-NYF is relatively coarse compared to those used in the aforementioned hind casts, but again, the consistency with Spence et al. (2014) was important. The perturbed atmosphere corresponds to their $W_{4^\circ S+15\%(62-70^\circ S)}$, which is an idealized poleward wind shift of 4°S and 15% intensification of westerly winds in the 62–70°S band. Such perturbation was guided by the results of 32 CMIP5 models under the RCP8.5 "business-as-usual" scenario (Spence et al., 2014). This methodology was used to correct the wind bias found in most present-day ("historical") CMIP5 simulations while keeping the wind shift and intensification throughout the 21st century. As the coastline is located southward of 70°S in the Amundsen Sea, it means that the coastal katabatic winds are unchanged in this perturbation. Moreover, only the wind field is perturbed, surface air temperature and humidity remain unchanged, which is justified by the lack of subsurface water sensitivity to these fields, as discussed by Spence et al. (2014). The corresponding global ocean under perturbed winds was also produced by Spence et al. (2014). All the global ocean simulations produced by Spence et al. (2014) are used after 100 years of spin-up under CORE-II-NYF. Importantly, no ice shelves are considered in their global ocean simulations, i.e., there is no cavity and the freshwater associated with ice-shelf melt is held constant and included in the climatological runoff injected into their ocean surface layer along the Antarctic coast.

Our present-day ice-shelf cavities have a geometry derived from year 2000 of the ice-sheet simulations from Cornford et al. (2015). The later are based on the BISICLES ice flow model, with basal friction coefficient and stiffening factor inverted to match the observed ice velocities. Present-day snow accumulation and oceanic melt rates are chosen to obtain the observed ice-sheet geometry. Their domain includes Dotson, Crosson, Thwaites, and Pine Island cavities. Their simulations use a bedrock/bathymetry that was built in a very similar way as ALBMAP (Le Brocq et al., 2010), with extra data from high-resolution airborne radar (Vaughan et al., 2006) and submarine surveys (Jenkins et al., 2010a), and including a pinning point underneath Thwaites (Cornford et al., 2015). It should be noted that the bedrock topography used in Cornford et al. (2015) is known to be inaccurate underneath Dotson and Crosson ice shelves (Millan et al., 2017). Our perturbed ice-shelf cavities have a geometry derived from year 2100 of one of the ice-sheet simulations from Cornford et al. (2015), namely their H/A/O"/F experiment which corresponds to one of their most extreme grounding line retreat for 2100. This simulation was forced by melt rates empirically derived from an ocean simulation with ice-shelf cavities and itself constrained by a CMIP3 model under the A1B emission scenario.

Table 1
Simulation Parameters

Name	Atmosphere and ocean forcing	Ice-shelf melt	Cavity geometry
AtmP_noIS	Spence's present	Zero	Cornford's present
AtmF_noIS	Spence's future	Zero	Cornford's present
AtmP	Spence's present	Interactive	Cornford's present
AtmF	Spence's future	Interactive	Cornford's present
AtmF_iceF	Spence's future	Interactive	Cornford's future

Note. See text for description of Spence and Cornford's results. "Interactive" melt refers to melt calculated through the three equations, while "Zero" means that melt is set to zero all along the simulation.

2.2. Regional Ocean Simulations

Our primary tool is the ocean model NEMO-3.6 (Nucleus for European Modelling of the Ocean) (Madec, 2016). The ice-shelf module in NEMO-3.6 was developed by Mathiot et al. (2017). NEMO includes sea ice dynamics and thermodynamics through the Louvain Ice Model (LIM3.6, Rousset et al., 2015). The regional model configuration, centered on the Amundsen Sea and referred to as AMU12.L75, was developed and evaluated with respect to observations in Jourdain et al. (2017). The resolution is quasi-isotropic, it is 1/12° in longitude and variable in latitude, equivalent to 2.4–4.2 km depending on the latitude, and 75 vertical levels are used with a thickness increasing from 1 m at the surface to 204 m at 6,000 m. The top and bottom cells have a thickness that varies to match the prescribed bathymetry and ice draft. As described by Jourdain et al. (2017), such resolution is sufficient to partially resolve mesoscale eddies in the deep ocean but it does not permit to resolve the Rossby radius on the continental shelf, and therefore does not represent the eddy contribution to the heat transport over the continental shelf (Stewart & Thompson, 2013). Our simulations do not account for tides, which are important in some regions as the Ross and Weddell sea (Flexas et al., 2015; Makinson et al., 2011). Tides could affect melt rates under Dotson ice-shelf according to Robertson (2013) but the presence of warm cavities in our simulations allows a circulation usually controlled by the melt-induced circulation rather than tides (Dutrieux et al., 2014; Robertson, 2013; Jourdain et al., 2017). Melt rates at ice-shelf bases are computed within the three equations from Hellmer and Olbers (1989); Holland and Jenkins (1999); and Jenkins et al. (2010b), with velocity-dependent transfer coefficients as in Mathiot et al. (2017) and Jourdain et al. (2017). The climatological monthly iceberg runoff produced by Merino et al. (2016) is prescribed in all our simulations. The 13th simulation year is analyzed throughout the paper, which is much longer than the model spin-up (Jourdain et al., 2017), and analyses of the 12th year give similar results (not shown).

Several comparisons to observational products were carried out in Jourdain et al. (2017): the simulated sea-ice seasonal cycle was within the interannual range of NSIDC (their Figure 3); compared to CTD measurements, the temperatures below 500 m on the continental shelf are overestimated by ∼0.5°C (their Figure 4), which is estimated to lead to an overestimation of melt rates by 15%; the ice shelf melt of Thwaites is within the observational range of uncertainty, while the ice shelf melt of Pine Island is overestimated by 9% (their Figure 5 and Table 1); the relationship between the volume and heat transport into the cavity and the melt rates compares reasonably well with those derived from in situ measurements (their Figure 9).

The five simulations used in this paper are shown in Table 1. In short, "AtmP" refers to Spence et al.'s (2014) present-day used for both our surface boundary conditions (i.e., radiative fluxes, surface air temperature

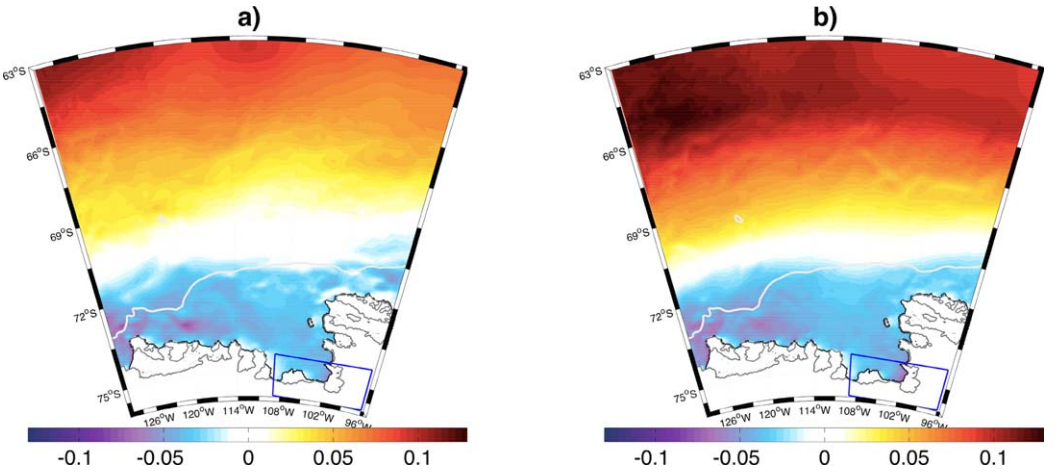

Figure 1. (a) Present annual mean zonal wind stress and (b) future annual mean zonal wind stress (N.m^{-2}). At these latitudes, wind is mostly zonal. The white line is the 1,500 m isobath and indicates the continental shelf break, and the black line corresponds to the ice-shelf fronts. All values are averaged over the 13th simulation year.

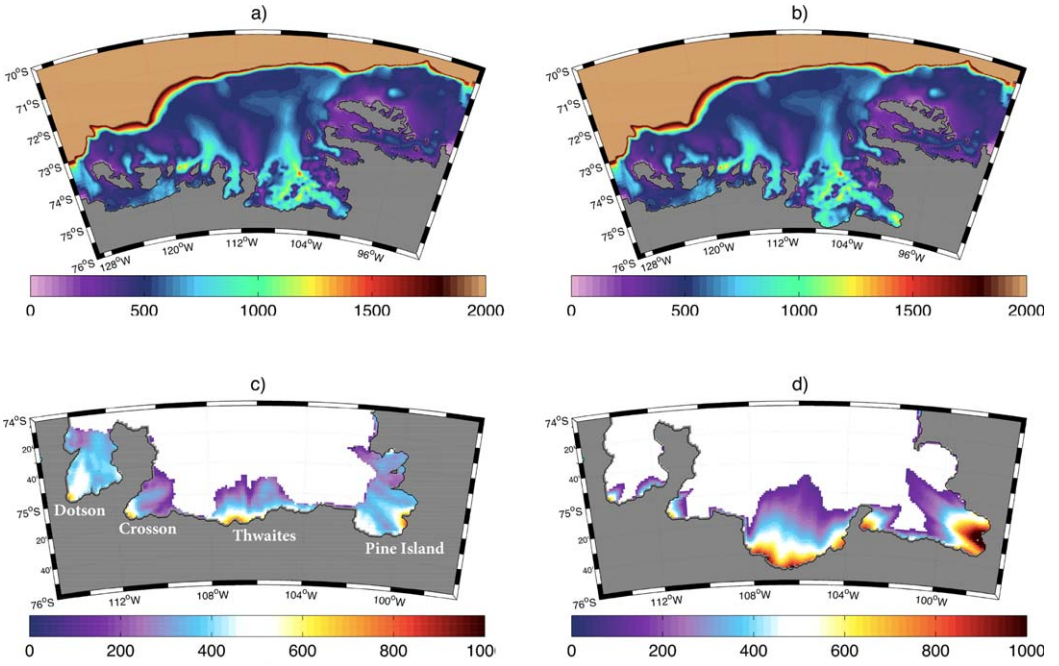

Figure 2. (a) Bathymetry (m) with present-day grounding lines, (b) bathymetry (m) with grounding lines estimated for 2100 (Cornford et al., 2015), (c) present-day ice draft depth (m) for Pine Island, Thwaites, Crosson, and Dotson, and (d) ice draft depth (m) estimated for 2100 (Cornford et al., 2015).

and humidity, precipitation, wind velocities) and our lateral boundary conditions (i.e., ocean temperature, salinity, velocities, sea ice fraction, and thickness), while "AtmF" refers to Spence et al.'s (2014) future simulation used for both our surface and lateral boundary conditions. The corresponding present and future zonal wind stress is represented in Figure 1. The wind perturbation is located north of the continental shelf break, as expected from a typical SAM anomaly (e.g., Spence et al., 2017, their supporting information Figure 1).

The ice-shelves geometry corresponds to Cornford et al.'s (2015) present-day in all our simulations except "AtmF_IceF" where the geometry comes from Cornford et al.'s (2015) simulation in 2100. In the region not represented in Cornford et al.'s (2015) domain, the bathymetry and ice-draft are the same as in Jourdain et al. (2017), i.e., based on BEDMAP2 (Figure 2). The calving threshold has been empirically chosen to 100 m (Cornford et al., 2015). The robustness of this threshold has been tested with a 300 m calving front, and the differences in basal melt rates are less than ∼10% under Thwaites and Pine Island.

In order to investigate the impact of interactive ice-shelf melt, two additional simulations are carried out, "AtmP_noIS" and "AtmF_noIS," where basal melt rates under ice shelves are set to zero. These two simulations are expected to produce results similar to Spence et al. (2014).

3. Results

3.1. Impact of Strengthened and Poleward Shifted Winds

In this subsection, we revisit the study by Spence et al. (2014) analyzing the effects of the SAM-like poleward wind shift, but in presence of interactive ice-shelf melt. To contrast the role of ice-shelves, we compare the ocean response to changing winds in presence of interactive ice-shelf melt (Figures 3a and 3c) and with zero ice-shelf melt (Figures 3b and 3d). With no ice-shelf melt, strengthened and poleward shifted winds induce a coastal ocean subsurface warming of about 0.4°C south of 72°S between 100°W and 120°W (Figure 3d). This result is close to the warming of about 0.5°C simulated by Spence et al. (2014) in this region (with no ice-shelves). The ocean subsurface response to modified winds in presence of interactive ice-shelf melt is very contrasted, with a coastal ocean subsurface temperature response of about −0.2°C south of 72°S between 100°W and 120°W (Figure 3c).

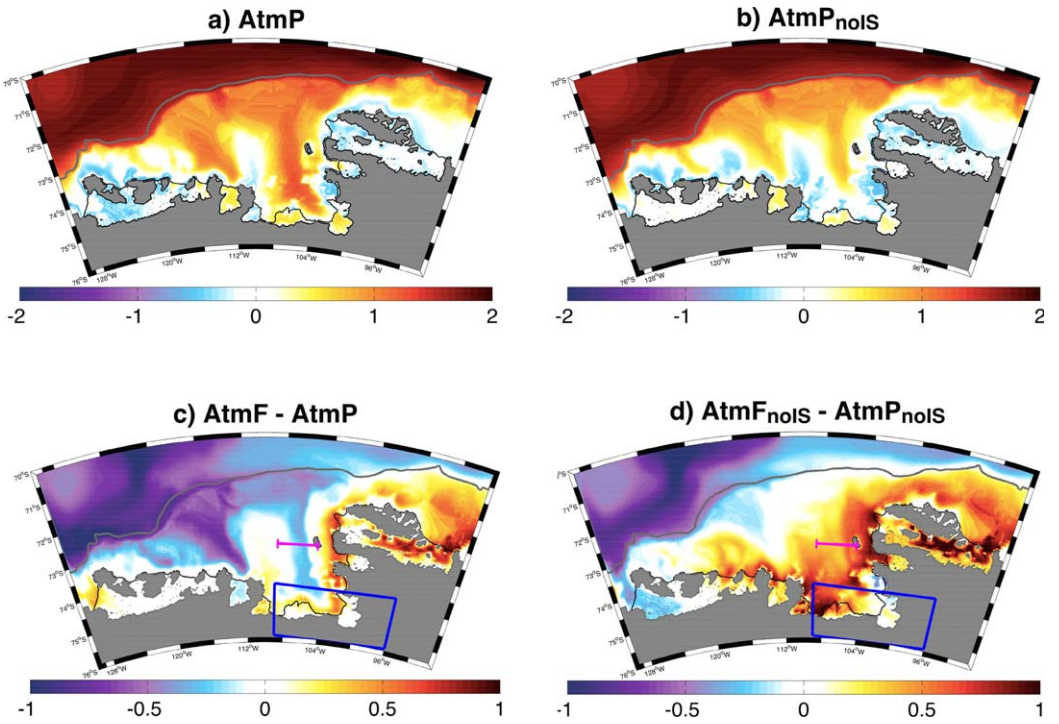

Figure 3. Conservative ocean temperature (°C) averaged over 200–1,000 m (annual mean over the 13th simulation year) in (a) AtmP and (b) AtmP_noIS. Wind-induced ocean temperature anomalies defined as (c) AtmF minus AtmP and (d) AtmF_noIS minus AtmP_noIS. The magenta line (73°S 105°W 109°W) is across the Pine Island Trough and is used to calculate horizontal transports in Figure 9. The blue box (76°S 74.3°S 96°W 109°W) is used throughout the paper to average vertical transport, temperatures, and heat budget terms near the fronts of Pine Island and Thwaites glaciers. The grey line represents the continental shelf break (1,500 m isobath).

We first briefly examine the mechanism with no ice shelf melt. As Spence et al. (2014), we find that the wind perturbation reduces or suppresses downward velocities over the continental shelf (Figures 4a and 4b), which raises the isotherms (Figures 5a and 5b) and leads to a subsurface warming through vertical advection (see heat budget terms in Figures 6c–6f). While the heat budget brings robust evidence that vertical heat advection explains the subsurface warming (this is the only positive term), the mechanism through which vertical heat advection is affected by the wind perturbation is complex. Wind has not been perturbed over the continental shelf in this area (Figure 1), but differences in sea ice fraction and sea ice motions (influenced by remote winds; Pope et al., 2017) affect Ekman pumping (Figure 6a). The moderate spatial correlation between vertical heat advection and Ekman pumping suggests that changes in subsurface temperature are partly explained by changes in Ekman pumping, itself resulting from changes in sea ice motions and coverage (Figure 6c). In average, the Amundsen Sea Embayment experiences reduced Ekman downwelling, so that the subsurface gets warmer. It is also possible that changes in sea ice production (Figure 6b) may affect vertical heat advection. While convection of dense water associated with brine rejection is parameterized through enhanced vertical diffusivity, this induces mixed-layer deepening or shoaling and affects lateral density gradients and therefore convergence/divergence, with possible effects on vertical motions (in a similar way as upward advection associated with ice-shelf melt). However, the non-significant spatial correlation between sea ice production and vertical heat advection (Figure 6c) does not support this mechanism. The pattern of horizontal heat advection is anticorrelated to the one of vertical advection (because Ekman downwelling is associated with divergence at depth), but horizontal heat advection if overall weaker and does not fully compensate vertical advection (Figure 6d). The mixing terms are also weaker than the advection terms, although not negligible (Figures 6e and 6f).

Finally, it should be noted that offshore subsurface waters (north of the continental shelf break) tend to cool in response to changing winds (Figure 3). A full heat budget analysis in the 200–1,000 m offshore layer shows that most of the cooling is explained by changes in horizontal advection, which mostly corresponds

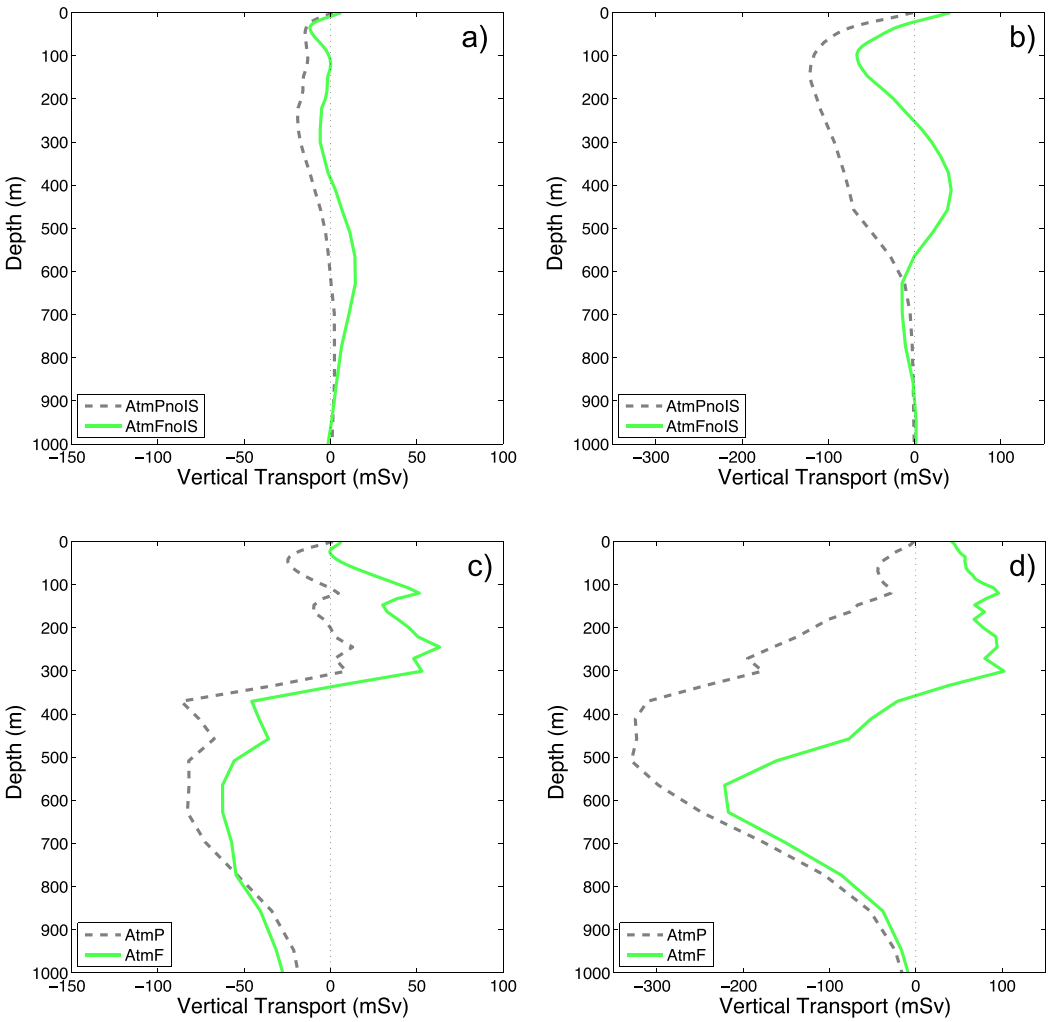

Figure 4. Vertical transport in mSv (for the 13th simulation year) in (a) AtmPnoIS and AtmFnoIS averaged over the blue box (76°S 74.3°S 96°W 109°W), (b) AtmPnoIS and AtmFnoIS averaged over the continental shelf (south of 72°S between 100°W and 120°W), (c) AtmP and AtmF averaged over the blue box (76°S 74.3°S 96°W 109°W), and (d) AtmP and AtmF averaged over the continental shelf (south of 72°S between 100°W and 120°W).

to the advection of Spence's remote anomaly by the ACC, as indicated by the negative anomaly along the western boundary in Figure 6d. There is also a smaller contribution from vertical advection (related to Ekman pumping) and vertical mixing offshore (not shown). The mechanism with no ice shelf melt is summarized in Figure 7a.

We now consider the response to the wind perturbation in presence of ice shelf cavities. In this case, summarized in Figure 7b, the response of Ekman pumping and sea ice production to changing wind is similar to the case with no ice-shelf melt over the continental shelf (Figure 8). The main difference is the presence of a melt-induced buoyancy-driven circulation in the ice shelf cavity, which can be referred to as ice-shelf or meltwater pumping. This circulation is strong enough to bring offshore waters onto the continental shelf (see net transport along the Pine Island Trough in Figure 9) and to create a deep downwelling in front of the ice shelf cavities (compare present-day vertical velocities with and without ice-shelf melt in Figure 4). Changes in vertical advection induced by the response of Ekman pumping to the wind perturbation still contribute to raise the isotherms (positive anomaly from vertical advection at depth in Table 2). But in presence of ice-shelf melt, this effect is overwhelmed by the horizontal advection (induced by the ice-shelf pump, see Figure 9) of colder offshore waters (cooled by the wind perturbation offshore) onto the continental shelf at depth (Figure 3c), which tends to lower the isotherms (Figures 5c and 5d). So overall, the wind perturbation cools the deep waters (below ~450 m) over the continental shelf (Figure 10b), and ice-shelf

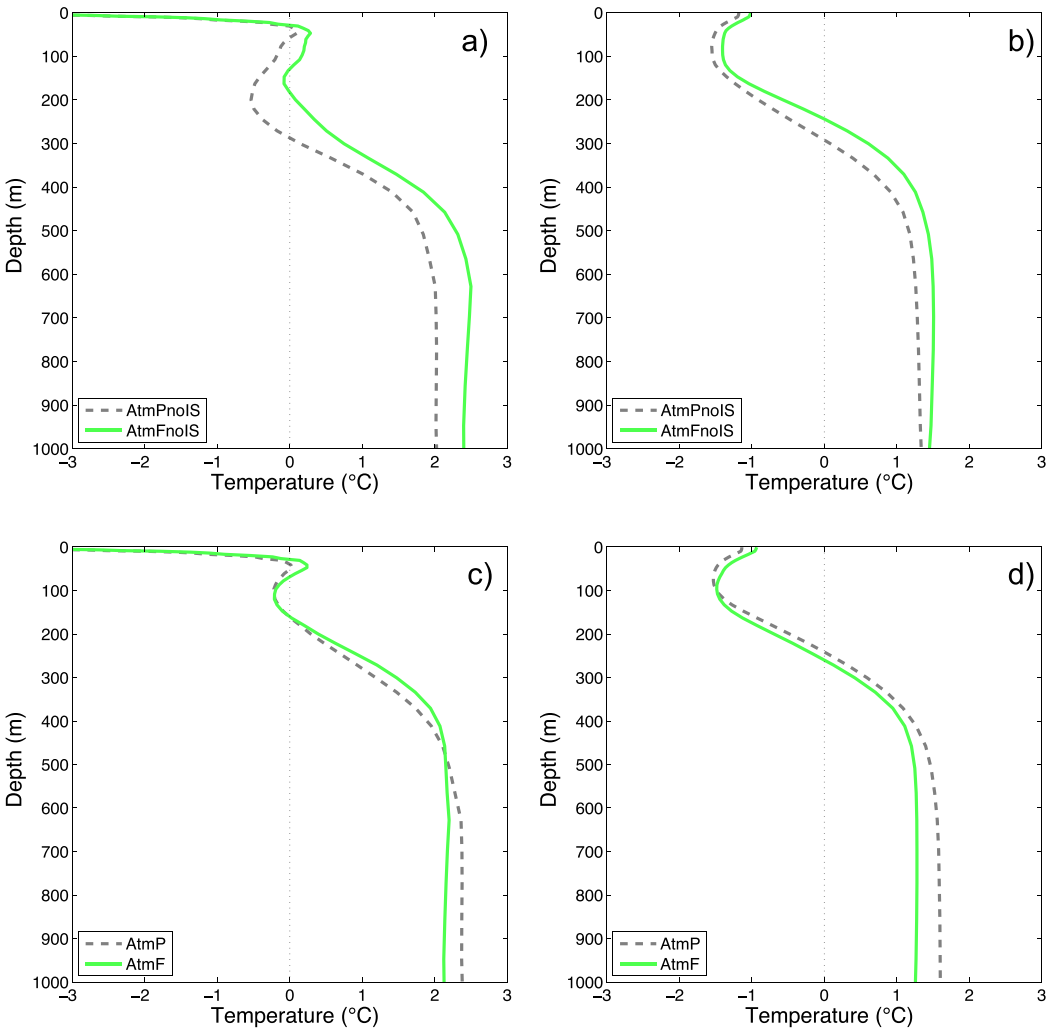

Figure 5. Conservative ocean temperature profiles in °C (for the 13th simulation year) in (a) AtmPnoIS and AtmFnoIS averaged over the blue box (76°S 74.3°S 96°W 109°W), (b) AtmPnoIS and AtmFnoIS averaged over the continental shelf: south of 72°S (100°W 120°W), (c) AtmP and AtmF averaged over the blue box (76°S 74.3°S 96°W 109°W), and (d) AtmP and AtmF averaged over the continental shelf: south of 72°S (100°W 120°W).

melt therefore decreases at depth (Figure 11). At intermediate depths, between 200 and 450 m, the advection of cold offshore water still dominates over large areas of the continental shelf (Figure 5d), but not in the vicinity of the ice shelf fronts where a warming is found in response to changing winds (Figures 10a and 5c). As in the case with no ice shelf melt, vertical advection induced by Ekman pumping near the ice-shelf fronts contributes to raise the isotherms in response to changing winds, with a slightly stronger effect in the intermediate layer (between 200 and 450 m) than in the deep layer (below 450 m) leading to an increased ice-shelf melt in the upper part of the cavities (Figure 11). Considering the entire cavities, the total meltwater flux increases by 6% and 21% for Pine Island and Thwaites, respectively. This increase meltwater flux leads to a stronger buoyancy-driven circulation that contributes to strengthen the upward velocity anomaly in front of the ice shelves in response to changing winds. Therefore, the ice-shelf buoyancy-driven circulation contributes to make the warming effect of vertical advection stronger than the cooling effect of horizontal advection in response to the wind perturbation. Such warming at intermediate depths is visible near several ice-shelf fronts in our domain but not farther away from the ice shelf fronts (Figure 10a). This mechanism, summarized in Figure 7b, is further confirmed by the online heat budget (Table 2). The response of horizontal and vertical advection to changing winds dominates the response of horizontal and vertical diffusion. Even if the latter is not negligible, it can be understood as an adjustment to the modified advection terms. It clearly appears that the warming effect of vertical advection overwhelms the cooling

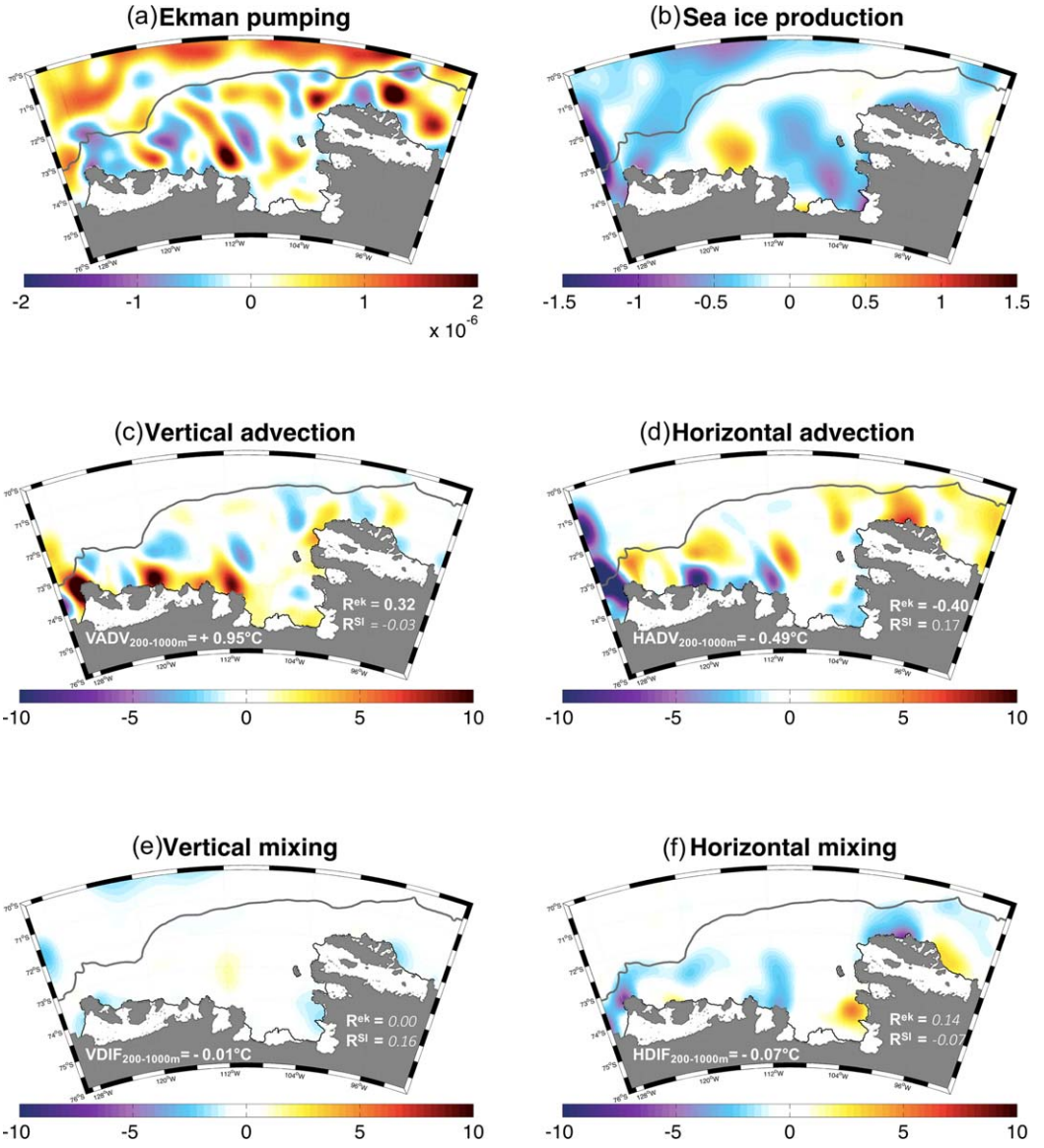

Figure 6. (a) Ekman pumping anomaly (m.s^{-1}) in the simulations with no ice shelf melt (AtmFnoIS minus AtmPnoIS), calculated from the total stress curl, i.e., accounting for the air/ocean, sea-ice/ocean, and bottom frictions (the later having a negligible effect, not shown). (b) Sea ice production anomaly (AtmFnoIS minus AtmPnoIS) in m.yr^{-1} averaged over the 13th simulation year. (c)–(f) Heat budget terms anomaly with no ice shelf melt (AtmFnoIS minus AtmPnoIS) averaged between 200 and 1,000 m depth. The terms of the heat budget were calculated online (i.e., calculated through the model equations every model time step), and accumulated from the beginning of the simulation to the 13th year to explain differences in the annual mean of the 13th year in two simulations (see equations (6) and (7) in Jourdain et al., 2017). The values in the lower left corner of plots (c)–(f) are the average over the continental shelf (south of 72°S and between 100°W and 120°W) between 200 and 1,000 m depth. The spatial correlation coefficients between Ekman pumping (R^{ek}) or sea ice production (R^{SI}) and the heat budget terms are indicated in (c)–(f). Bold R are significant at 99% (i.e., $p < 0.01$), while italic R are nonsignificant at 90% (i.e., $p > 0.10$). All fields have been smoothed using a Gaussian filter of $\sigma = 30$ km. Correlations are calculated from the filtered variables, but accounting for the associated decrease in number of degrees of freedom in the calculation of significance.

effect of horizontal advection in response to changing winds in the intermediate layer, with a reversed effect in the deep layer.

A striking feature in Figure 10a is the warm anomaly along the coast. At first glance, this could appear as a warm anomaly coming from the eastern lateral boundary of our domain and propagating westward and southward along the coast, advected by the part of the coastal current closely following the coastline. If so,

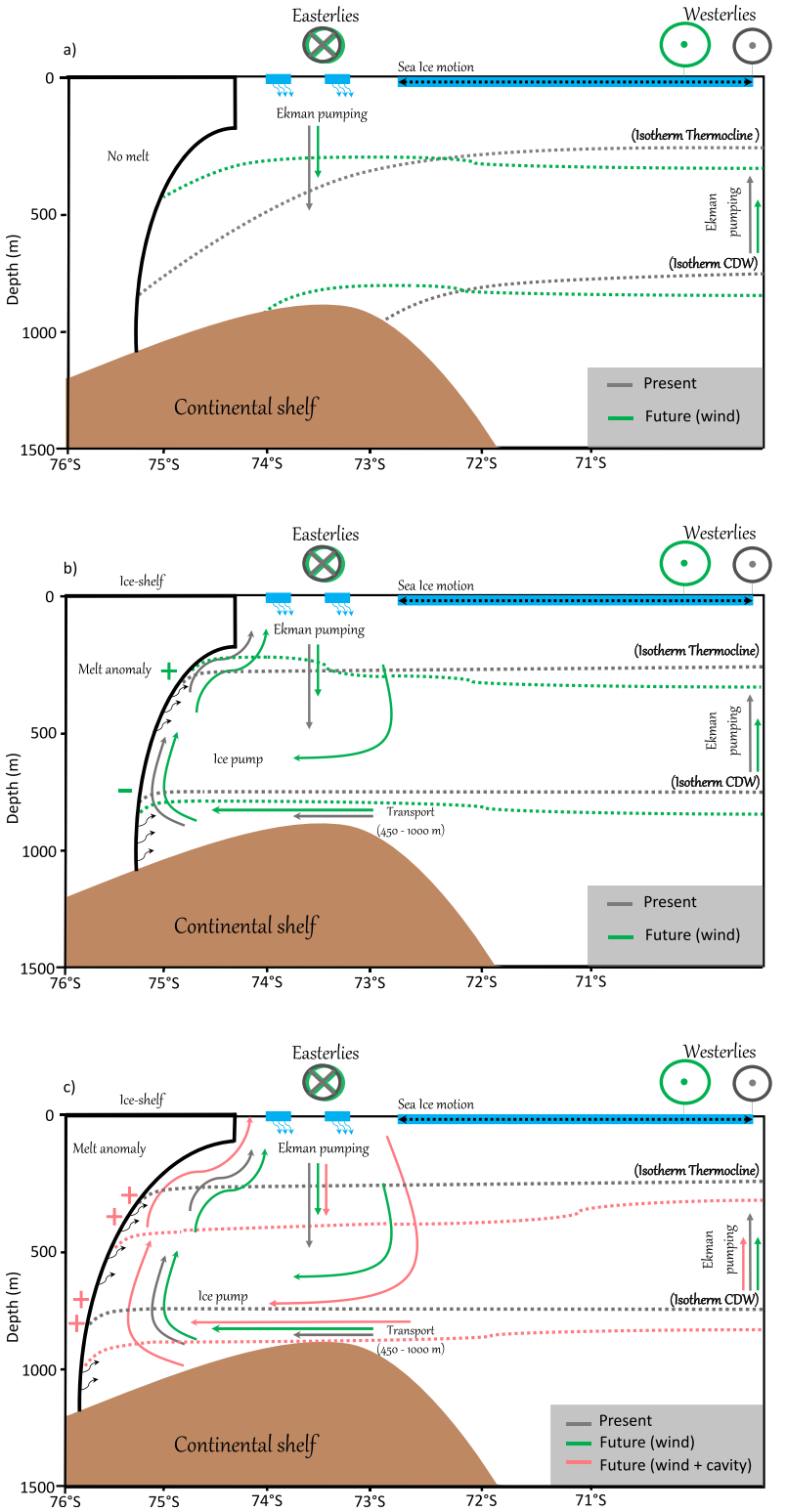

Figure 7. Schematic of the ocean and ice-shelf melt responses to changing winds without interactive ice-shelf melt (a), with interactive ice-shelf melt (b) and with interactive ice-shelf melt and grounding line retreat (c). Straight arrows represent the ocean mass transport. Grey arrows and isotherms correspond to the "present" (without shifted winds), while green arrows and isotherms correspond to the "future" (with shifted winds) and pink arrows and isotherms correspond to the "future" (with shifted wind and grounding line retreat). Cooling (warming) at a given depth is visible as deepening (or shoaling) of isotherms. The wind has not been perturbed over the continental shelf and changes in Ekman pumping result from differences in sea ice motions and coverage. Horizontal arrows represent deep onshore transport induced by the melt-induced buoyancy-driven circulation.

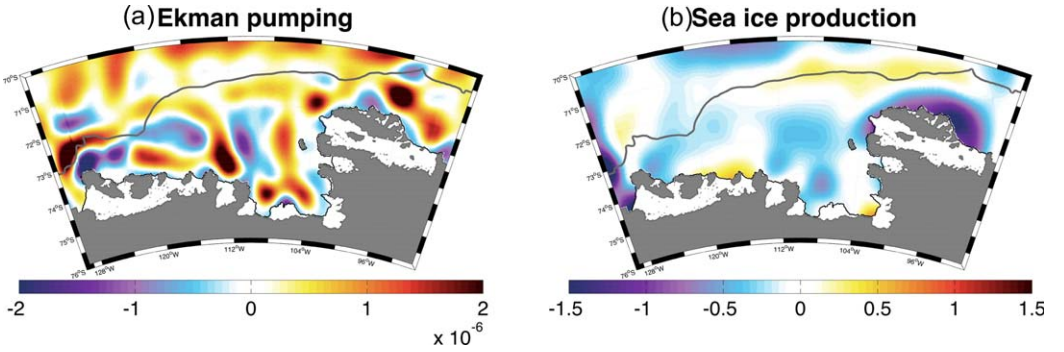

Figure 8. (a) Ekman pumping anomaly (m.s^{-1}) in the simulations with ice shelf melt (AtmF minus AtmP), calculated from the total stress curl, i.e., accounting for the air/ocean, sea-ice/ocean, and bottom frictions (the later having a negligible effect, not shown). (b) Sea ice production anomaly (AtmF minus AtmP) in m.yr^{-1}. All values are averaged over the 13th simulation year.

such anomaly would be questionable because the anomaly from the adjacent Bellingshausen Sea simulated by Spence et al. (2014) has not accounted for the presence of ice shelves. However, the negative contribution of horizontal advection in the heat budget presented in Table 2 indicates that heat advection by the current closely following the coastline cannot be responsible for the warming found along the coast. Nonetheless, to better evaluate the influence of the eastern open boundary, we have run two additional simulations (with and without ice-shelf melt) with no temperature and salinity anomalies along the eastern boundary. This yields similar anomalies over the continental shelf as in the other simulations (not shown) indicating that (1) the advection of water from the Bellingshausen Sea by the coastal current plays a minor role in the simulated ocean response to changing winds, and (2) our results are not affected by the anomalies produced by Spence et al. (2014) in the adjacent coastal Bellingshausen Sea. It should be noted that the relatively large warm anomaly in response to changing winds found near the eastern boundary of our domain (Figure 10a) causes important effect on melt rates underneath Abbot, with a total melt increased by almost a factor of three. This is nonetheless unlikely to affect our results on Thwaites and Pine Island, because additional simulations in which melt rates were forced to zero underneath Abbot gave a very similar sensitivity to the wind perturbation for Thwaites and Pine Island (the melt rate sensitivity to the wind was changed by less than 2%, not shown).

Overall, the effect of strengthened and poleward shifting wind on melt rates is relatively moderate, with 21% increase in total subice-shelf melt underneath Thwaites and 6% underneath Pine Island. In comparison, observation-based melt rates underneath Pine Island have a relative standard deviation of 41% at the

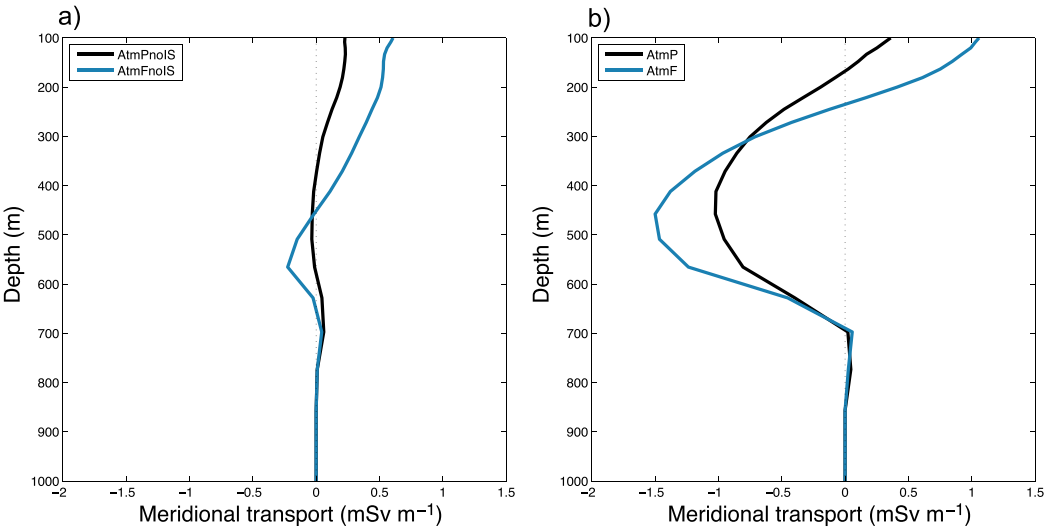

Figure 9. Net horizontal transport through the magenta section (see Figure 3) in mSv.m^{-1}. Negative values represent southward transport. All values are averaged over the 13th simulation year.

Table 2
Heat Budget Terms Anomaly in Presence of Ice Shelf Melt (AtmF minus AtmP) in the Blue Box (Excluding Ice-Shelf Cavities)

Layer	Horizontal advection (°C)	Vertical advection (°C)	Horizontal mixing (°C)	Vertical mixing (°C)	Δ T (°C)
200–450 m	−3.00	+3.81	−0.40	−0.27	+0.15
450–1,000 m	−2.01	+1.88	−0.70	+0.69	−0.15

Note. The terms of the heat budget were calculated online (i.e., calculated through the model equations every model time step), and accumulated from the beginning of the simulation to the 13th year to explain differences in the annual mean of the 13th year in two simulations (see equations (6) and (7) in Jourdain et al., 2017). All numbers have been calculated with all digits and are here displayed with two digits, so they may not seem to exactly add up.

interannnual time scale (calculated from Dutrieux et al., 2014). Moreover, it is unclear to what extent increased melt rates in the upper part of the cavity and decreased melt rates in the deepest part can actually trigger instability of glacier flows. Previous studies on marine ice-sheet instabilities have indeed examined the glaciers response to stronger melt increase at depth (e.g., Favier et al., 2014; Joughin et al., 2014). Alternatively, or additionally, the glaciers retreat observed in the Amundsen Sea sector (Mouginot et al., 2014; Rignot et al., 2014) may result from climatic perturbations from the past (Christianson et al., 2016; Smith et al., 2017). In this case, it is essential to test the sensitivity of subice-shelf melt to the evolving shape of ice-shelf cavities. This is the focus of the next subsection.

3.2. Ice-Shelf Melt Response to Changing Ice Dynamics

In this subsection, we consider another "future" state, namely AtmF_iceF, in which, in addition to perturbed winds, the ice-draft is derived from year 2100 of Cornford et al.'s (2015) simulation with one of their most extreme grounding line retreats. Comparing AtmF to AtmF_iceF indicates the effect of changing cavity shape, while comparing AtmP to AtmF_iceF gives the combined effect of changing winds and changing ice draft. As in the previous subsection, we focus on Thwaites and Pine Island.

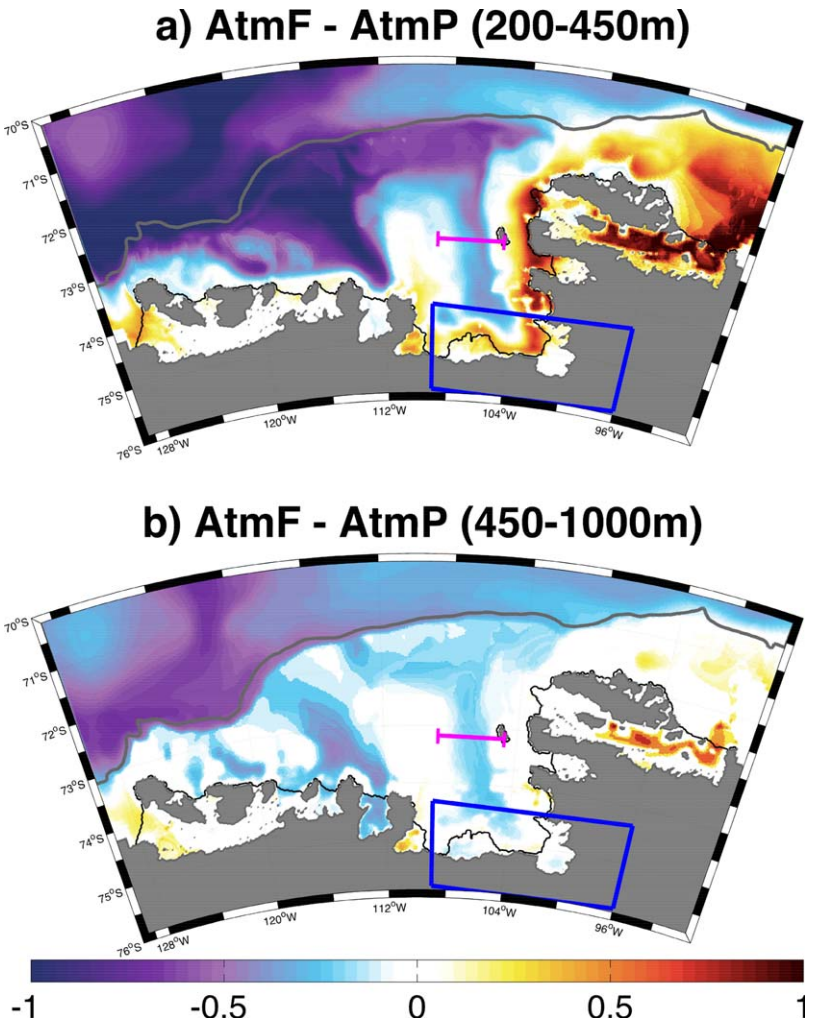

Figure 10. Conservative ocean temperature anomalies in degree Celsius (AtmF minus AtmP) averaged over (a) 200–450 m, (b) 450–1,000 m and over the 13th simulation year. The grey contour represents the 1,500 m isobath.

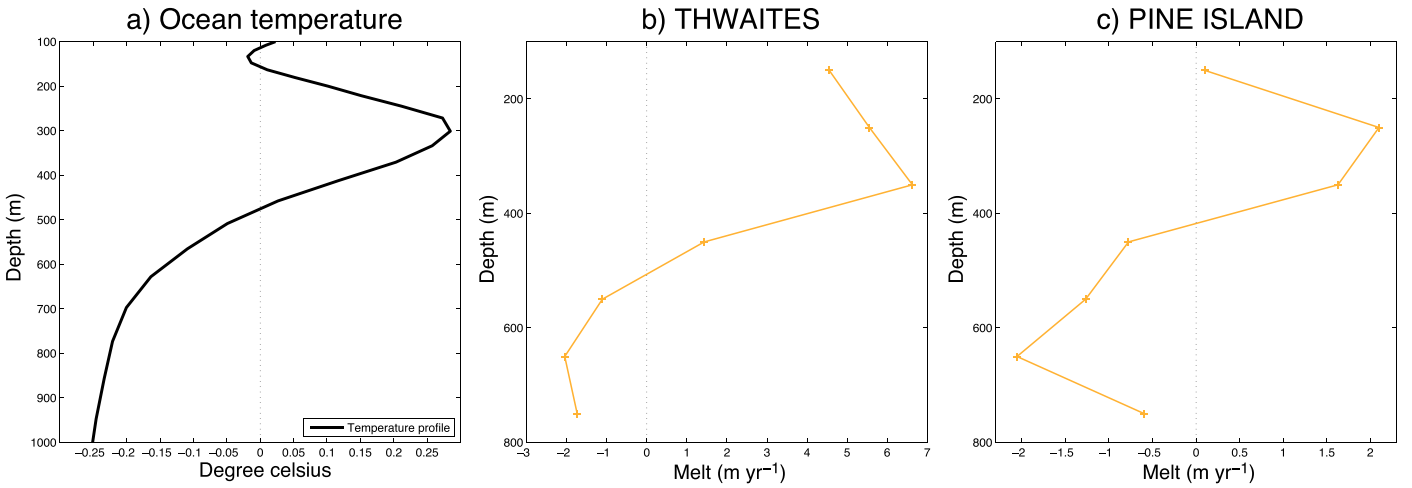

Figure 11. (a) Conservative ocean temperature profile anomaly (AtmF minus AtmP) near Pine Island and Thwaites glacier fronts (i.e., blue box in Figure 3, excluding ice shelves). (b) Ice-shelf melt rate (m yr^{-1}) anomaly (AtmF minus AtmP) under Pine Island and (c) under Thwaites. All values are averaged over the 13th simulation year.

Because of the retrograde bedrock under Thwaites and Pine Island glaciers, retreated grounding lines in AtmF_iceF cause deeper cavities than in AtmP and AtmF, so the ice area exposed to warm CDW increases (Figure 7). Therefore the larger ocean/ice interface at depths affected by CDW causes a much larger total melt flux (in $Gt.yr^{-1}$) below ~600 m in AtmF_iceF compared to AtmF (Figures 12c and 12d). The larger exposed area alone cannot directly explain the large increase in average melt rates (in $m.yr^{-1}$) almost everywhere along the ice drafts (Figures 12a and 12b). This is rather an indirect effect whereby a larger ocean/ice interface creates more melt and therefore a stronger buoyancy-driven circulation within the cavity (Figures 12e and 12f), which increases heat exchange at the ice/ocean interface. This process acts as a positive feedback on melt rates and is summarized in Figure 7c. It is important to notice that such feedback is only present because we use a velocity-dependent melt parameterization (see next section and Dansereau et al., 2014). The strengthened circulation is partly compensated by a decreased thermal forcing all along the ice-draft (Figures 12g and 12h). This decreased thermal forcing is not directly due to the injection of cold meltwater, because the flux of entrained warm deep water throughout the Amundsen Sea cavities is 100 to 500 times more important than the melt water flux itself, and overall, the thermal effect of entrainment overwhelms the thermal effect of injecting water at the freezing point (Jourdain et al., 2017). Another explanation can be found in the melt-induced circulation. As shown in the previous subsection, melting underneath Pine Island and Thwaites induces a divergence at depth in the cavities, which leads to the advection of offshore subsurface waters (CDW or modified CDW) onto the continental shelf as well as a deep downwelling in front of the cavities. Both AtmF and AtmF_IceF have the same wind-induced cooling of offshore subsurface waters between 200–1,000 m, so the decreased thermal forcing cannot be related to changes in the temperature of offshore waters. By contrast, the deep downwelling induced by the ice-shelf pump brings cold waters from upper layers downward and into the cavity, so the much stronger melt rates in AtmF_IceF lead to stronger deep downwelling in front of the cavities and therefore explain the colder temperatures in front of the ice shelves and a weaker thermal forcing in AtmF_IceF (Figures 12 and 13). This is also visible through the isotherms in Figure 7c.

As the ice shelves get thinner, the area covered by the ice/ocean interface also becomes larger at low depths. This explains the significantly larger total melt flux near the ocean surface in AtmF_iceF compared to AtmF (Figures 12c and 12d), and it can be the opposite for mid-depths, like near 400 m for Pine Island (Figure 12d). Interestingly, the thermal forcing in the upper part of the cavities is less affected than in the deepest part (Figures 12g and 12h), while the larger melt amounts at depth could have been expected to bring more buoyant cold water toward the upper part. Possible explanations for this are (i) the buoyant plume entrains warm water which can overwhelm the direct cooling effect of injecting water at the freezing point (Jourdain et al., 2017), and (ii) if the ice shelf gets thinner, it can be more affected by warm waters that are found in summer above the thermocline.

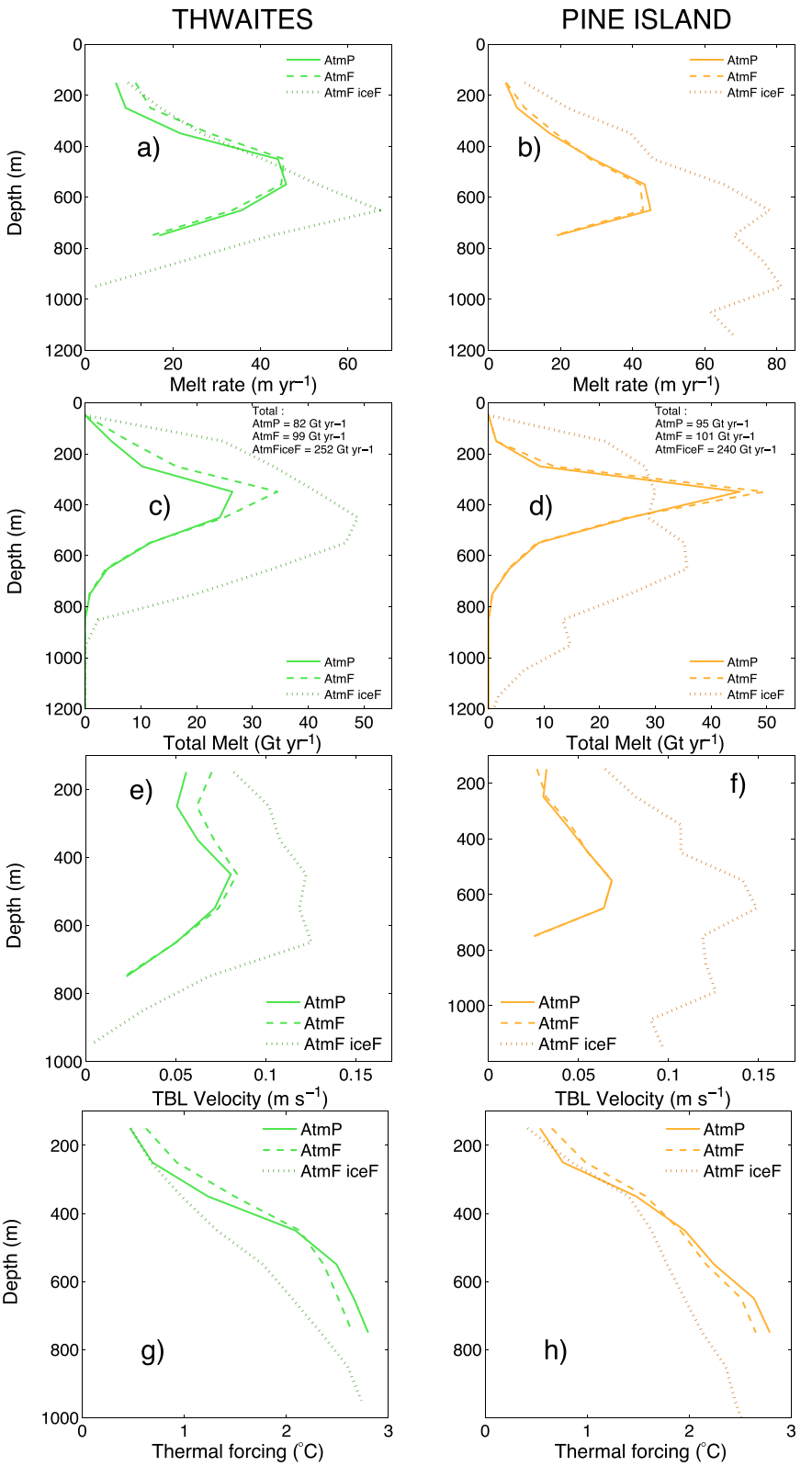

Figure 12. (a and b) Mean basal melt rate in m yr^{-1}; (c and d) total basal melt rate in Gt yr^{-1}; (e and f) top-boundary-layer velocity in in m s^{-1}; and (g and h) top-boundary-layer thermal forcing in °C profiles in function of the depth from the surface in AtmP, AtmF, and AtmF_iceF simulations, for Thwaites (left) and Pine Island (right). The top boundary layer is defined as a 30 m ocean layer below the ice draft, and all profiles are averaged over 100 m bins.

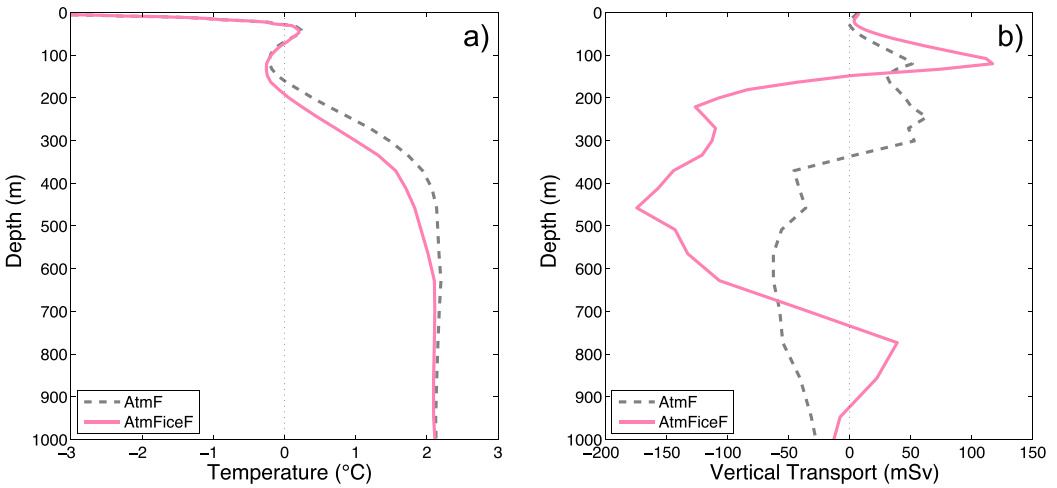

Figure 13. (a) Conservative ocean temperature profiles (°C) averaged over the blue box (76°S 74.3°S 96°W 109°W) (b) Vertical transport in mSv averaged over the blue box for AtmF and AtmFiceF simulations (13th simulation year mean).

Overall, prescribing a strong grounding line retreat leads to total melt fluxes multiplied by ∼2.5, and to local melt rates typically multiplied by 2–3 below 600 m. Comparing AtmF_iceF to AtmF clearly shows that this effect is only due to a change in cavity shapes. To confirm this result, we have run another simulation with present-day winds and retreated ice geometry, and we have obtained very similar results (not shown). Our estimates emphasize the potential for strong feedbacks between the ocean and the ice dynamics, which is a strong incentive to couple ocean models to ice sheet models. Nonetheless, our values are to be considered with care, because the grounding line retreats that we used is likely largely overestimated and may actually be representative of much later than 2100 (see next section). Our estimates only hold for strong grounding line retreats without considering the likelihood of such event in a world where atmosphere, ocean, sea ice, and ice shelves are connected by feedbacks. Therefore, these values should not be compared to the aforementioned effects of changing winds, because Spence et al. (2014) and Cornford et al. (2015) did not build their scenarios in a fully coupled ocean/ice-sheet model and did not see the exact same climate perturbations.

4. Discussion and Conclusions

In this paper, we have analyzed the ocean response to strengthened and poleward shifted winds using the NEMO-3.6 ocean model in a regional configuration centered on the Amundsen Sea. From our numerical simulation, we show that the coastal ocean response to perturbed winds is strongly impacted by the circulation induced by ice-shelf melt. Changing winds cause coastal ocean temperature changes leading to increase total melt underneath Pine Island and Thwaites by 6% and 21%, respectively. Such modeled total melt increase is relatively trifling compared to the increase by a factor of ∼2.5 induced by an extreme future grounding line retreat and related positive feedback due to a stronger melt-induced circulation.

Perturbed winds (in the presence of ice-shelves) cause a subsurface cooling over the continental shelf through advection of offshore waters that are projected to cool by the end of 21st century in Spence et al.'s (2014) simulations. However, it is unclear what would be the future temperature trend of offshore CDW. First, Spence et al.'s (2014) scenario only accounts for the SAM trend. Even if El Niño Southern Oscillation is not expected to be directly responsible for trends in the Southern Ocean (Jones et al., 2016; Scambos et al., 2017), interannual and decadal variability in the Tropical Pacific induces temperature variability in the Amundsen Sea (Steig et al., 2012) and could be more important than trends for the Amundsen Sea because they could trigger irreversible grounding line retreat (Jenkins et al., 2016; Smith et al., 2017). Remote processes occurring as far as in the Northern subpolar regions may also affect CDW properties, and results from the CMIP5 models indicate a CDW warming from 0.33°C to 0.41°C over the 21st century depending on the emission scenario (Sallée et al., 2013). These numbers are highly uncertain given that global climate models are significantly biased over the Southern Ocean (e.g., Little & Urban, 2016) and some important

components of the Earth system are missing (e.g., no ice-shelf cavities in CMIP5 models). This is nonetheless in agreement with oceanographic observations since the 1990s that also indicate a warming trend of ~0.05°C per decade for the CDW located northward of the Amundsen Sea (Schmidtko et al., 2014). It should therefore be stressed that our study only accounts for the regional effect of strengthened and poleward shifting winds related to the SAM trend and a need for improving our current understanding of the influence of climate modes of variability on the climatology of coastal winds is emphasized. It is also important to note that our conclusions should not be extrapolated to other regions like East Antarctica where there are limited intrusions of CDW onto the continental shelf and melt rates are weaker than in the Amundsen Sea. One more limitation is the absence of tides and eddies in our simulations which are important processes that can bring heat onto the continental shelf (Flexas et al., 2015; Makinson et al., 2011; Robertson, 2013; Stewart & Thompson, 2013). As explained in Jourdain et al. (2017), our resolution partially resolves the mesoscale eddies in the deep ocean (Hallberg, 2013) and the mean flow-topography interactions involved in the CDW transport onto the continental shelf (Assmann et al., 2013; Nakayama et al., 2014; St-Laurent et al., 2013) but we do not resolves the baroclinic Rossby radius of deformation over the continental-shelf, and our simulations are missing relevant wind-driven coastal ocean dynamics (Millot & Crépon, 1981).

Despite these limitations, our study clearly shows the importance of considering ice shelves in ocean modelling works. Indeed, the conclusions drawn by Spence et al. (2014) that the entire Amundsen Sea subsurface would warm in response to strengthened and poleward shifted winds is invalid when the ocean circulation induced by ice shelf melt is represented. Our results suggest that the coastal warming found in simulations with no representation of ice shelves is potentially wrong. The results from ice-sheet modeling studies using parameterized melt rates from temperature at the nearest climate model grid points (see examples in the Introduction) are therefore also questionable as ice-shelf cavities have so far never been considered in the CMIP climate models.

To evaluate the potential feedback of grounding line retreat onto the ocean circulation and ice shelf melt, we have used an ice-sheet simulation producing a strong grounding line retreat for 2100 (Cornford et al., 2015). The melt response to changing winds is only +21% (+17 Gt.yr^{-1}) and +6% (+6 Gt.yr^{-1}) for Thwaites and Pine Island, respectively, when the cavity shape and grounding line position are unchanged, but it becomes +207% (+170 Gt.yr^{-1}) and +153% (+145 Gt.yr^{-1}) when the cavity shape and grounding line position change to Cornford et al.'s (2015) estimate for 2100. These values have to be considered with caution, because the bedrock topography used is known to be very inaccurate (Millan et al., 2017), and the total basal melt computation depends largely on the bathymetry used (Schodlok et al., 2012). The methodologies used by Spence et al. (2014) and Cornford et al. (2015) to estimate their future state while accounting for model limitations are also not completely consistent with each other even though both aim to represent the end of the 21st century under a strong emission scenario.

Notwithstanding the above limitations, our sensitivity experiments clearly indicate that accounting for evolving grounding line and cavity shape is potentially of primary importance for climate projections. Schodlok et al. (2012) also reported a significant sensitivity to the cavity geometry, with ~25% difference in melt rates under Pine Island between two different bathymetry data sets. By contrast, Seroussi et al. (2017) did not notice any significant change in melt rates as Thwaites retreated in their ice/ocean coupled simulations. Two explanations are proposed for the difference between our results and Seroussi et al. (2017). First of all, melt rates in Seroussi et al. (2017) are less extreme than those used by Cornford et al. (2015), leading to a grounding line retreat of ~20 km in 2050 in Seroussi et al. (2017), compared to ~70 km in 2100 in Cornford et al.'s (2015) H/A/O″/F experiment used in our study. It could therefore be argued that Cornford et al.'s (2015) 2100 may be representative of much later than 2100, although the grounding line response is nonlinear in time, in particular on a retrograde bedrock (see the 240 km retreat in 2200 in Cornford et al.'s, 2015, Figure 7). The second important difference between Seroussi et al. (2017) and our study is not related to the scenario, but rather to the parameters used in the three-equation melt rate formulation. In their ocean simulations, Seroussi et al. (2017) used a velocity-independent formulation of melt rates, while we use the velocity-dependent version (e.g., Dansereau et al., 2014; Holland & Jenkins, 1999). As discussed in the previous section, the velocity profiles (Figures 12e and 12f) underneath Pine Island and Thwaites suggest a feedback whereby the melt-induced ocean circulation further strengthens melt rates. Such feedback would only be simulated with a velocity-dependent formulation. To assess the importance of this feedback, we have rerun two additional simulations, both with velocity-independent formulation, both with present-

Table 3
Cavity Melt Rate ($Gt.yr^{-1}$) for Present-Day Winds, Ice Drafts Representative of Either 2000 or 2100, and Either Velocity-Dependent or Velocity-Independent Melt Formulations

	Ice draft 2000 velocity-dep.	Ice draft 2100 velocity-dep.	Ice draft 2000 velocity-ind.	Ice draft 2100 velocity-ind.
Pine Island	95	252	67	83
Thwaites	82	260	44	103

Note. Annual means over the 13th year of simulations are shown.

day winds, and with ice shelf drafts representative of the years 2000 and 2100. The exchange velocities are chosen as 2.27 10^{-5} and 6.37 10^{-7} $m.s^{-1}$ for heat and salt, respectively. The results are summarized in Table 3. Using a velocity-independent formulation, the melt increase for a larger cavity is relatively weaker than using a velocity-dependent formulation (+23% compared to +165% for Pine Island and +134% compared to +217% for Thwaites). Given that turbulence in the TBL depends on shear and therefore on ocean velocities, a velocity-dependent formulation is expected to better represent TBL processes than a velocity-dependent formulation, at least if the ocean circulation is well represented. This suggests that velocity-dependent formulation should be used in ocean/ice-sheet coupled models to simulate important grounding line retreats.

To conclude, our results are a strong incentive to use ocean/ice sheet coupled models to assess basal melt rates and their evolutions for reliable estimations of the contribution of West Antarctica to the global sea level rise over the 21st century and beyond. The presence of ice-shelf cavities and evolving cavities into ocean model is therefore necessary to proper estimate basal melt rates. Importantly, velocity-dependent melt formulations represent feedbacks that are significantly weaker with velocity-independent formulations. The fact that relatively coarse ocean models may not accurately represent the circulation underneath ice shelves is therefore another challenging aspects of ice sheet modeling embedded in global climate projections (Nowicki et al., 2016). Furthermore, melt parameterizations used in ice sheet models (Asay-Davis et al., 2017) would need to account for such feedback. Again, our results only concern the Amundsen Sea, and the potential importance of ocean/ice sheet coupling at a century scale might be different in other regions of Antarctica.

Acknowledgments
This work was funded by the French National Research Agency (ANR) through the TROIS-AS (ANR-15-CE01-0005-01) project. M.D., N.J., G.D., and J.L. are part of Labex OSUG2020 (ANR10 LABX56). N.J. is an Associate Investigator of the ARC Centre of Excellence for Climate System Science. P.S. was supported by an Australian Research Council (ARC) DECRA Fellowship (DE150100223). The computational resources were provided by CINES through the egi6035 and gge6066 projects. We thank P. Mathiot and G. Madec for the development of the ice-shelf module which is central in this work, and S. Cornford for making his data available. The model code for NEMO-3.6 is available from the NEMO website (www.nemo-ocean.eu). The branch used in this study is the development branch named dev_r5151_UKMO_ISF at revision 5932.

References

Asay-Davis, X. S., Jourdain, N. C., & Nakayama, Y. Developments in simulating and parameterizing interactions between the Southern Ocean and the Antarctic Ice sheet. *Current Climate Change Reports*, *3*, 316–329.

Assmann, K., Jenkins, A., Shoosmith, D., Walker, D., Jacobs, S., & Nicholls, K. (2013). Variability of circumpolar deep water transport onto the Amundsen Sea continental shelf through a shelf break trough. *Journal of Geophysical Research: Oceans*, *118*, 6603–6620. https://doi.org/10.1002/2013JC008871

Bintanja, R., Van Oldenborgh, G., Drijfhout, S., Wouters, B., & Katsman, C. (2013). Important role for ocean warming and increased ice-shelf melt in Antarctic sea-ice expansion. *Nature Geoscience*, *6*(5), 376–379.

Bracegirdle, T. J., Shuckburgh, E., Sallee, J.-B., Wang, Z., Meijers, A. J., Bruneau, N., . . . Wilcox, L. J. (2013). Assessment of surface winds over the Atlantic, Indian, and Pacific Ocean sectors of the Southern Ocean in CMIP5 models: Historical bias, forcing response, and state dependence. *Journal of Geophysical Research: Atmospheres*, *118*, 547–562. https://doi.org/10.1002/jgrd.50153

Bracegirdle, T. J., Turner, J., Hosking, J. S., & Phillips, T. (2014). Sources of uncertainty in projections of twenty-first century westerly wind changes over the Amundsen Sea, west Antarctica, in CMIP5 climate models. *Climate Dynamics*, *43*, 2093–2104.

Chen, G., & Held, I. M. (2007). Phase speed spectra and the recent poleward shift of southern hemisphere surface westerlies. *Geophysical Research Letters*, *34*, L21805. https://doi.org/10.1029/2007GL031200

Christianson, K., Bushuk, M., Dutrieux, P., Parizek, B. R., Joughin, I. R., Alley, R. B., . . . Holland, D. M. (2016). Sensitivity of Pine Island glacier to observed ocean forcing. *Geophysical Research Letters*, *43*, 10,817–10,825. https://doi.org/10.1002/2016GL070500

Cornford, S. L., Martin, D. F., Payne, A. J., Ng, E. G., Le Brocq, A. M., Gladstone, R. M., . . . Vaughan, D. G. (2015). Century-scale simulations of the response of the west Antarctic ice sheet to a warming climate. *The Cryosphere Discussions*, *9*, 1887–1942.

Dansereau, V., Heimbach, P., & Losch, M. (2014). Simulation of sub-ice shelf melt rates in a general circulation model: Velocity-dependent transfer and the role of friction. *Journal of Geophysical Research: Oceans*, *119*, 1765–1790. https://doi.org/10.1002/2013JC008846

Deconto, R. M., & Pollard, D. (2016). Contribution of Antarctica to past and future sea-level rise. *Nature*, *531*, 591–597.

De Rydt, J., & Gudmundsson, G. H. (2016). Coupled ice shelf-ocean modeling and complex grounding line retreat from a seabed ridge. *Journal of Geophysical Research: Earth Surface*, *121*, 865–880. https://doi.org/10.1002/2015JF003791

Dinniman, M. S., Klinck, J. M., & Smith, W. O. (2011). A model study of Circumpolar Deep Water on the West Antarctic Peninsula and Ross Sea continental shelves. *Deep Sea Research Part II: Topical Studies in Oceanography*, *58*(13), 1508–1523.

Dutrieux, P., De Rydt, J., Jenkins, A., Holland, P. R., Ha, H. K., Lee, S. H., . . . Schröder, M. (2014). Strong sensitivity of Pine Island ice-shelf melting to climatic variability. *Science*, *343*(6167), 174–178.

Favier, L., Durand, G., Cornford, S., Gudmundsson, G., Gagliardini, O., Gillet-Chaulet, F., . . . Le Brocq, A. (2014). Retreat of Pine Island glacier controlled by marine ice-sheet instability. *Nature Climate Change*, *4*(2), 117–121.

Flexas, M. D M., Schodlok, M. P., Padman, L., Menemenlis, D., & Orsi, A. H. (2015). Role of tides on the formation of the Antarctic slope front at the Weddell-Scotia confluence. *Journal of Geophysical Research: Oceans*, *120*, 3658–3680. https://doi.org/10.1002/2014JC010372

Fogt, R. L., & Wovrosh, A. J. (2015). The relative influence of tropical sea surface temperatures and radiative forcing on the Amundsen Sea low. *Journal of Climate*, *28*(21), 8540–8555.

Gille, S. T. (2008). Decadal-scale temperature trends in the southern hemisphere ocean. *Journal of Climate*, *21*(18), 4749–4765.

Gillett, N. P., Arora, V. K., Zickfeld, K., Marshall, S. J., & Merryfield, W. J. (2011). Ongoing climate change following a complete cessation of carbon dioxide emissions. *Nature Geoscience*, *4*(2), 83–87.

Gillett, N. P., & Fyfe, J. (2013). Annular mode changes in the CMIP5 simulations. *Geophysical Research Letters*, *40*, 1189–1193. https://doi.org/10.1002/grl.50249

Golledge, N. R., Kowalewski, D. E., Naish, T. R., Levy, R. H., Fogwill, C. J., & Gasson, E. G. (2015). The multi-millennial Antarctic commitment to future sea-level rise. *Nature*, *526*(7573), 421–425.

Griffies, S. M., Biastoch, A., Böning, C., Bryan, F., Danabasoglu, G., Chassignet, E. P., . . . Yin, J. (2009). Coordinated ocean-ice reference experiments (cores). *Ocean Modelling*, *26*(1), 1–46.

Hallberg, R. (2013). Using a resolution function to regulate parameterizations of oceanic mesoscale eddy effects. *Ocean Modelling*, *72*, 92–103.

Hartmann, D. L., & Lo, F. (1998). Wave-driven zonal flow vacillation in the southern hemisphere. *Journal of the Atmospheric Sciences*, *55*(8), 1303–1315.

Hellmer, H., & Olbers, D. (1989). A two-dimensional model for the thermohaline circulation under an ice shelf. *Antarctic Science*, *1*(4), 325–336.

Holland, D. M., & Jenkins, A. (1999). Modeling thermodynamic ice-ocean interactions at the base of an ice shelf. *Journal of Physical Oceanography*, *29*(8), 1787–1800.

Jacobs, S., Jenkins, A., Hellmer, H., Giulivi, C., Nitsche, F., Huber, B., & Guerrero, R. (2012). The Amundsen Sea and the Antarctic ice sheet. *Oceanography*, *25*(3), 154–163.

Jenkins, A., Dutrieux, P., Jacobs, S. S., McPhail, S. D., Perrett, J. R., Webb, A. T., & White, D. (2010a). Observations beneath Pine Island glacier in west Antarctica and implications for its retreat. *Nature Geoscience*, *3*(7), 468–472.

Jenkins, A., Dutrieux, P., Jacobs, S., Steig, E. J., Gudmundsson, G. H., Smith, J., & Heywood, K. J. (2016). Decadal ocean forcing and Antarctic ice sheet response: Lessons from the Amundsen Sea. *Oceanography*, *29*(4), 106–117.

Jenkins, A., Nicholls, K. W., & Corr, H. F. (2010b). Observation and parameterization of ablation at the base of Ronne ice shelf, Antarctica. *Journal of Physical Oceanography*, *40*(10), 2298–2312.

Jones, J. M., Gille, S. T., Goosse, H., Abram, N. J., Canziani, P. O., Charman, D. J., . . . Eisenman, I. *et al.* (2016). Assessing recent trends in high-latitude southern hemisphere surface climate. *Nature Climate Change*, *6*(10), 917–926.

Joughin, I., Smith, B. E., & Holland, D. M. (2010). Sensitivity of 21st century sea level to ocean-induced thinning of Pine Island glacier, Antarctica. *Geophysical Research Letters*, *37*, L20502. https://doi.org/10.1029/2010GL044819

Joughin, I., Smith, B. E., & Medley, B. (2014). Marine ice sheet collapse potentially under way for the Thwaites glacier basin, west Antarctica. *Science*, *344*(6185), 735–738.

Jourdain, N. C., Mathiot, P., Merino, N., Durand, G., Le Sommer, J., Spence, P., . . . Madec, G. (2017). Ocean circulation and sea-ice thinning induced by melting ice shelves in the Amundsen sea. *Journal of Geophysical Research: Oceans*, *122*, 2550–2573. https://doi.org/10.1002/2016JC012509

Le Brocq, A. M., Payne, A. J., & Vieli, A. (2010). An improved Antarctic dataset for high resolution numerical ice sheet models (albmap v1). *Earth System Science Data*, *2*(2), 247–260.

Large, W., & Yeager, S. (2009). The global climatology of an interannually varying air–sea flux data set. *Climate Dynamics*, *33*(2–3), 341–364.

Limpasuvan, V., & Hartmann, D. L. (1999). Eddies and the annular modes of climate variability. *Geophysical Research Letters*, *26*(20), 3133–3136.

Little, C. M., & Urban, N. M. (2016). CMIP5 temperature biases and 21st century warming around the Antarctic coast. *Annals of Glaciology*, *57*(73), 69–78.

Madec, G. (2016). *The nemo ocean engine, note du pole de modelisation* (Vol. 27). Paris, France: Institut Pierre-Simon Laplace (IPSL). Retrieved from http://www.nemo-ocean.eu/About-NEMO/Reference-manuals

Makinson, K., Holland, P. R., Jenkins, A., Nicholls, K. W., & Holland, D. M. (2011). Influence of tides on melting and freezing beneath Filchner-Ronne ice shelf, Antarctica. *Geophysical Research Letters*, *38*, L06601. https://doi.org/10.1029/2010GL046462

Marshall, G. J. (2003). Trends in the southern annular mode from observations and reanalyses. *Journal of Climate*, *16*(24), 4134–4143.

Martin, M., Winkelmann, R., Haseloff, M., Albrecht, T., Bueler, E., Khroulev, C., & Levermann, A. (2011). The potsdam parallel ice sheet model (pism-pik)–part 2: Dynamic equilibrium simulation of the Antarctic ice sheet. *The Cryosphere*, *5*(3), 727–740.

Mathiot, P., Jenkins, A., Harris, C., & Madec, G. (2017). Explicit and parametrized representation of under ice shelf seas in a z* coordinate ocean model. *Journal Geoscientific Model Development*, *10*, 2849–2874.

Merino, N., Le Sommer, J., Durand, G., Jourdain, N. C., Madec, G., Mathiot, P., & Tournadre, J. (2016). Antarctic icebergs melt over the Southern Ocean: Climatology and impact on sea-ice. *Ocean Modelling*, *104*, 99–110.

Millan, R., Rignot, E., Bernier, V., Morlighem, M., & Dutrieux, P. (2017). Bathymetry of the Amundsen Sea Embayment sector of West Antarctica from operation IceBridge gravity and other data. *Geophysical Research Letters*, *44*, 1360–1368. https://doi.org/10.1002/2016GL072071

Millot, C., & Crépon, M. (1981). Inertial oscillations on the continental shelf of the Gulf of Lions: Observations and theory. *Journal of Physical Oceanography*, *11*, 639–657.

Mouginot, J., Rignot, E., & Scheuchl, B. (2014). Sustained increase in ice discharge from the Amundsen Sea embayment, west Antarctica, from 1973 to 2013. *Geophysical Research Letters*, *41*, 1576–1584. https://doi.org/10.1002/2013GL059069

Nakayama, Y., Menemenlis, D., Schodlok, M., & Rignot, E. (2017). Amundsen and Bellingshausen seas simulation with optimized ocean, sea ice, and thermodynamic ice shelf model parameters. *Journal of Geophysical Research: Oceans*, *122*, 6180–6195. https://doi.org/10.1002/2016JC012538

Nakayama, Y., Timmermann, R., Schröder, M., & Hellmer, H. (2014). On the difficulty of modeling circumpolar deep water intrusions onto the Amundsen Sea continental shelf. *Ocean Modelling*, *84*, 26–34.

Nowicki, S. M., Payne, A., Larour, E., Seroussi, H., Goelzer, H., Lipscomb, W., . . . Shepherd, A. (2016). Ice sheet model intercomparison project (iCMIP6) contribution to cmip6. *Geoscientific Model Development*, *9*(12), 4521–4545.

Pauling, A. G., Bitz, C. M., Smith, I. J., & Langhorne, P. J. (2016). The response of the southern ocean and Antarctic sea ice to freshwater from ice shelves in an earth system model. *Journal of Climate*, *29*(5), 1655–1672.

Pope, J. O., Holland, P. R., Orr, A., Marshall, G. J., & Phillips, T. (2017). The impacts of El Niño on the observed sea ice budget of west Antarctica. *Geophysical Research Letters*, *44*, 6200–6208. https://doi.org/10.1002/2017GL073414

Raphael, M., Marshall, G., Turner, J., Fogt, R., Schneider, D., Dixon, D., . . . Hobbs, W. (2016). The Amundsen Sea low: Variability, change, and impact on Antarctic climate. *Bulletin of the American Meteorological Society*, *97*(1), 111–121.

Rignot, E., Mouginot, J., Morlighem, M., Seroussi, H., & Scheuchl, B. (2014). Widespread, rapid grounding line retreat of Pine Island, Thwaites, smith, and Kohler glaciers, west Antarctica, from 1992 to 2011. *Geophysical Research Letters*, *41*, 3502–3509. https://doi.org/10.1002/2014GL060140

Robertson, R. (2013). Tidally induced increases in melting of Amundsen Sea ice shelves. *Journal of Geophysical Research: Oceans*, *118*, 3138–3145. https://doi.org/10.1002/jgrc.20236

Rousset, C., Vancoppenolle, M., Madec, G., Fichefet, T., Flavoni, S., Barthélemy, A., . . . Vivier, F. (2015). The Louvain-la-Neuve Sea ice model lim3. 5: Global and regional capabilities. *Geoscientific Model Development Discussions*, *8*(4), 3403–3441.

Sallée, J.-B., Shuckburgh, E., Bruneau, N., Meijers, A. J., Bracegirdle, T. J., Wang, Z., & Roy, T. (2013). Assessment of Southern ocean water mass circulation and characteristics in cmip5 models: Historical bias and forcing response. *Journal of Geophysical Research: Oceans*, *118*, 1830–1844. https://doi.org/10.1002/jgrc.20135

Scambos, T. A., Bell, R. E., Alley, R. B., Anandakrishnan, S., Bromwich, D. H., Brunt, K., . . . Yager, P. L. (2017). How much, how fast?: A science review and outlook for research on the instability of Antarctica's Thwaites glacier in the 21st century. *Global and Planetary Change*, *153*, 16–34.

Schmidtko, S., Heywood, K. J., Thompson, A. F., & Aoki, S. (2014). Multidecadal warming of Antarctic waters. *Science*, *346*(6214), 1227–1231.

Schodlok, M. P., Menemenlis, D., Rignot, E., & Studinger, M. (2012). Sensitivity of the ice-shelf/ocean system to the sub-ice-shelf cavity shape measured by Nasa Ice bridge in pine island glacier, west Antarctica. *Annals of Glaciology*, *53*(60), 156–162.

Schoof, C. (2007). Ice sheet grounding line dynamics: Steady states, stability, and hysteresis. *Journal of Geophysical Research*, *112*, F03S28. https://doi.org/10.1029/2006JF000664

Seroussi, H., Nakayama, Y., Larour, E., Menemenlis, D., Morlighem, M., Rignot, E., & Khazendar, A. (2017). Continued retreat of Thwaites glacier, west Antarctica, controlled by bed topography and ocean circulation. *Geophysical Research Letters*, *44*, 6191–6199. https://doi.org/10.1002/2017GL072910

Shepherd, A., Ivins, E. R., Geruo, A., Barletta, V. R., Bentley, M. J., Bettadpur, S., . . . Jay Zwally, H. (2012). A reconciled estimate of ice-sheet mass balance. *Science*, *338*(6111), 1183–1189.

Smith, J. A., Andersen, T. J., Shortt, M., Gaffney, A. M., Truffer, M., Stanton, T. P., . . . Vaughan, D. G. (2017). Sub-ice-shelf sediments record history of twentieth-century retreat of pine island glacier. *Nature*, *541*(7635), 77–80.

Spence, P., Griffies, S. M., England, M. H., Hogg, A. M., Saenko, O. A., & Jourdain, N. C. (2014). Rapid subsurface warming and circulation changes of antarctic coastal waters by poleward shifting winds. *Geophysical Research Letters*, *41*, 4601–4610. https://doi.org/10.1002/2014GL060613

Spence, P., Holmes, R. M., Hogg, A. M., Griffies, S. M., Stewart, K. D., & England, M. H. (2017). Localized rapid warming of west Antarctic subsurface waters by remote winds. *Nature Climate Change*, *7*, 595–603.

Steig, E. J., Ding, Q., Battisti, D., & Jenkins, A. (2012). Tropical forcing of circumpolar deep water inflow and outlet glacier thinning in the Amundsen Sea embayment, west Antarctica. *Annals of Glaciology*, *53*(60), 19–28.

Stewart, A. L., & Thompson, A. F. (2013). Connecting antarctic cross-slope exchange with southern ocean overturning. *Journal of Physical Oceanography*, *43*(7), 1453–1471.

St-Laurent, P., Klinck, J. M., & Dinniman, M. S. (2013). On the role of coastal troughs in the circulation of warm circumpolar deep water on Antarctic shelves. *Journal of Physical Oceanography*, *43*, 51–64.

St-Laurent, P., Klinck, J., & Dinniman, M. (2015). Impact of local winter cooling on the melt of Pine Island glacier, Antarctica. *Journal of Geophysical Research: Oceans*, *120*, 6718–6732. https://doi.org/10.1002/2015JC010709

Swart, N., & Fyfe, J. (2012). Observed and simulated changes in the southern hemisphere surface westerly wind-stress. *Geophysical Research Letters*, *39*, L16711. https://doi.org/10.1029/2012GL052810

Swart, N., & Fyfe, J. (2013). The influence of recent Antarctic ice sheet retreat on simulated sea ice area trends. *Geophysical Research Letters*, *40*, 4328–4332. https://doi.org/10.1002/grl.50820

Thoma, M., Jenkins, A., Holland, D., & Jacobs, S. (2008). Modelling circumpolar deep water intrusions on the Amundsen Sea continental shelf, Antarctica. *Geophysical Research Letters*, *35*, L18602. https://doi.org/10.1029/2008GL034939

Thompson, D. W., & Wallace, J. M. (2000). Annular modes in the extratropical circulation. Part i: Month-to-month variability*. *Journal of Climate*, *13*(5), 1000–1016.

Turner, J., Orr, A., Gudmundsson, G. H., Jenkins, A., Bingham, R. G., Hillenbrand, C.-D., & Bracegirdle, T. J. (2017). Atmosphere-ocean-ice interactions in the Amundsen Sea embayment, west Antarctica. *Reviews of Geophysics*, *55*, 235–276. https://doi.org/10.1002/2016RG000532

Turner, J., Phillips, T., Hosking, J. S., Marshall, G. J., & Orr, A. (2013). The Amundsen Sea low. *International Journal of Climatology*, *33*(7), 1818–1829.

Vaughan, D. G., Corr, H. F., Ferraccioli, F., Frearson, N., O'hare, A., Mach, D., . . . Young, D. A. (2006). New boundary conditions for the west Antarctic ice sheet: Subglacial topography beneath pine island glacier. *Geophysical Research Letters*, *33*, L09501. https://doi.org/10.1029/2005GL025588

Wåhlin, A. K., Muench, R. D., Arneborg, L., Björk, G., Ha, H. K., Lee, S. H., & Alsén, H. (2012). Some implications of Ekman layer dynamics for cross-shelf exchange in the Amundsen sea. *Journal of Physical Oceanography*, *42*, 1461–1474.

Yin, J., Overpeck, J. T., Griffies, S. M., Hu, A., Russell, J. L., & Stouffer, R. J. (2011). Different magnitudes of projected subsurface ocean warming around Greenland and Antarctica. *Nature Geoscience*, *4*(8), 524–528.

Zheng, F., Li, J., Clark, R. T., & Nnamchi, H. C. (2013). Simulation and projection of the southern hemisphere annular mode in CMIP5 models. *Journal of Climate*, *26*(24), 9860–9879.